Journal of Alloys and Compounds 495 (2010) 173–180

Contents lists available at ScienceDirect

Journal of Alloys and Compounds

journal homepage: www.elsevier.com/locate/jallcom

Preparation and characterization of sol–gel derived sodium–potassium bismuth titanate powders and thick films deposited by screen printing

Haibo Zhang[a,b,*], Shenglin Jiang[a], Koji Kajiyoshi[b]

[a] Department of Electronic Science and Technology, Huazhong University of Science and Technology, Wuhan, 430074, China
[b] Research Laboratory of Hydrothermal Chemistry, Faculty of Science, Kochi University, 2-5-1, Akebono, Kochi, 780-8520, Japan

ARTICLE INFO

Article history:
Received 29 October 2009
Received in revised form 18 January 2010
Accepted 20 January 2010
Available online 1 February 2010

Keywords:
Sodium–potassium bismuth titanate
Lead-free piezoelectric
Sol–gel
Thick films
Ferroelectric properties
Piezoelectric properties

ABSTRACT

$Bi_{0.5}(Na_{0.82}K_{0.18})_{0.5}TiO_3$ (NKBT) lead-free thick films have been successfully deposited on Pt electroded alumina substrates using screen printing from the sol–gel derived powders. Fourier transform infrared (FT-IR) spectroscopy, differential thermal analysis (DTA), thermogravimetric analysis (TG) and X-ray diffraction (XRD) were used to characterize the process of crystallization. The cubic shape particulates of the order of 140–260 nm in size can be obtained by calcining the xerogel at 650 °C, and there is no obvious agglomeration of the NKBT powders. The resulting typical 90 μm thick NKBT films sintered at 1140 °C exhibit relative dielectric constant of 836 (at 10 kHz), dielectric constant of 2.9%, remanent polarization of 25.6 $\mu C/cm^2$, coercive field of 69.3 kV/cm, and longitudinal effective piezoelectric coefficient, d_{33eff} of 95 pm/V. The improvement of the electric properties can be attributed to the larger domain wall density and less domain wall pinning resulting from the increased film thickness of NKBT thick films.

1. Introduction

The research on lead-free piezoelectric materials has become more and more concentrated in the last few years due to the environmental issues arising from the lead toxicity [1]. Bismuth sodium titanate, $(Bi_{0.5}Na_{0.5})TiO_3$ (NBT), is considered to be an excellent candidate as a key lead-free piezoelectric material and discovered by Smolenskii et al. [2]. NBT exhibits relatively large remanent polarization of $P_r = 38\ \mu C/cm^2$, and a high coercive field of $E_c = 73$ kV/cm at room temperature, and the strong ferroelectricity of NBT-based solid solution is attributed to $(Bi_{0.5}Na_{0.5})^{2+}$ ions, especially Bi^{3+} ions, of A-site on perovskite structure (ABO_3) [3,4]. It has been reported that NBT ceramics modified with $BaTiO_3$ (BT) [5] or $Bi_{0.5}K_{0.5}TiO_3$ (KBT) [6] showed improved dielectric and piezoelectric properties because there exists the corresponding rhombohedral tetragonal morphotropic phase boundary (MPB). Many studies have been conducted to research on the NBT-based binary and ternary systems with MPB [5,7,8]. Among these systems, the NBT–KBT system which was first reported by Sasaki et al., [9] show a high piezoelectric response due to the MPB between rhombohedral NBT and tetragonal KBT. In previous studies [10,11], we have prepared NKBT lead-free piezoelectric thick films by screen printing from the solid state reaction, the high remanent polarization and longitudinal effective piezoelectric coefficient, d_{33eff} have been obtained. However, NBT-based ceramics or thick films are commonly produced by the conventional milling of starting oxides followed by the solid state reaction. The resulting powders prepared by this method usually have serious agglomeration and inhomogeneous particle size as a result of the high temperature reaction. The drawbacks of the solid state reaction were inhomogeneous mixing, irregular morphology, larger particle size, broader particle size distribution, and loss of the volatile Bi, K and Na element, and high energy consumption.

Recently, the so-called "chemical solution method" have been widely attracting attention [12]. The use of precursor solution leads to more homogeneous and reactive powders that densify at lower temperatures limiting in this way the loss of volatile Bi, K and Na element. Several chemical solution methods, such as conventional sol–gel [12], hydrothermal synthesis [13], stearic acid gel [14], and mechanochemical synthesis [15] were applied for the preparation of NBT-based ceramics. Among these methods the sol–gel process is a popular chemical method for the preparation of fine powders and ceramic coatings and this process offers low capital investment cost. In addition, the sol–gel method presents several advantages for coatings processing the control of composition, surface morphology engineering and low-temperature processing, which allows the use of thermally fragile substrates, are its principal merits. Therefore, in the present study we employ the sol–gel process to prepare NKBT powders at lower temperature for limiting the loss of volatile Bi_2O_3 K_2O and Na_2O, which is beneficial for maintaining of high performance of the NKBT thick films.

* Corresponding author.
E-mail address: changhb@gmail.com (H. Zhang).

0925-8388/$ – see front matter.
doi:10.1016/j.jallcom.2010.01.114

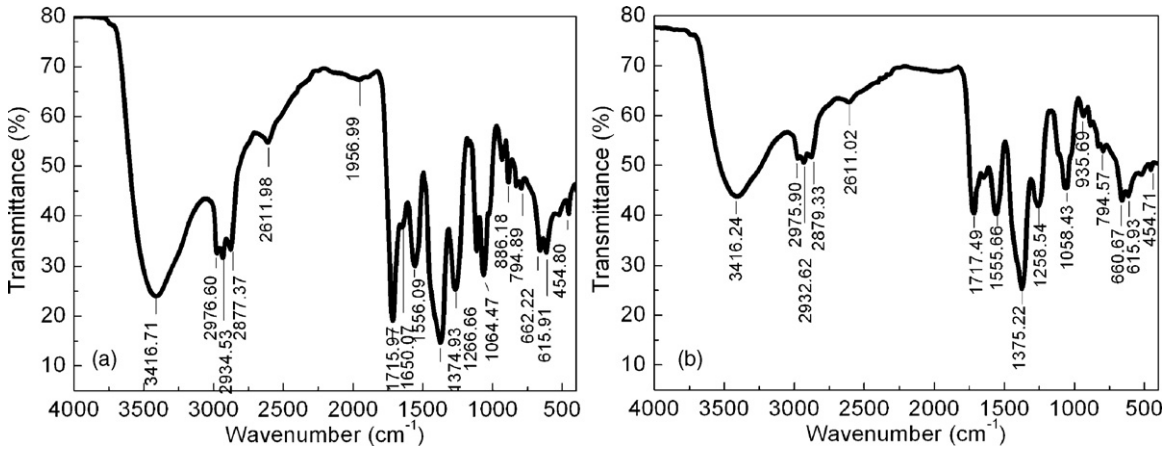

Fig. 1. FT-IR spectra of the NKBT precursors after heat treatment at 100 °C (a) and 160 °C (b) for 2 h.

Most recently, piezoelectric thick films with thickness in the range of 10–100 μm have attracted significant attention. They have been widely applied to micropumps, ultrasonic motors, resonators, microfluidic separators, high frequency transducers, and energy harvesting [16,17], because they exhibit properties such as larger displacement and quick response, high frequency, and can be precisely controlled [17]. However, the thick films are difficult to produce using lapping and machining bulk ceramics due to the expense, waste and difficulty in handling the ceramics, on the other hand, most of the thin film processing, such as sol–gel, sputtering, physical vapour deposition, chemical vapour deposition, and pulsed laser deposition are not practical due to the slow deposition rates and high levels of stress generated during processing which can lead to cracking of the film [18]. The thick film technologies filled the gap between bulk materials and thin films. Many studies have been reported on the preparation of piezoelectric thick films by screen printing, tape casting, composite sol–gel, electrophoretic deposition, ink-jet printing, and aerosol deposition [16]. Among these methods, screen printing technology has an advantage in that it enables low-cost fabrication of a device and device arrays in desired pattern without a photolithography.

One goal of this work was to establish the better synthesis parameters to produce NKBT fine powders by sol–gel processing. Another goal of the present work is preparation and characterization of NKBT lead-free piezoelectric thick films by screen printing from the sol–gel derived NKBT powders. In addition, the dielectric, ferroelectric and piezoelectric properties of the optimum NKBT thick films sintered at various temperatures are investigated.

2. Experimental procedure

Sodium acetate ($(CH_3COO)Na{\cdot}3H_2O$), potassium acetate ($(CH_3COO)K$), bismuth nitrate ($Bi(NO_3)_3{\cdot}5H_2O$), tetrabutyl titanate ($Ti(OC_4H_9)_4$), glacial acetic acid (CH_3COOH), and triethanolamine ($N(C_2H_4OH)_3$) were used as starting materials. Sodium acetate, potassium acetate, and bismuth nitrate were dissolved in glacial acetic acid (CH_3COOH) and triethanolamine was added as a catalyst. Triethanolamine (TEA, $N(C_2H_4OH)_3$) is an alkanolamine which can complex with transition metal to form stable complex [19] to avoid any rapid hydrolysis and condensation in existence of water [20]. Tetrabutyl titanate was dissolved in glycol ether and acetylacetone was used to stabilize the solution, all above reagents were at analytic purity. NKBT precursor solutions were prepared by mixed the above two solutions according to chemical formula $Bi_{0.5}(Na_{0.82}K_{0.18})_{0.5}TiO_3$, and the concentration of solution was controlled to 0.4–0.6 mol/L by diluting with methoxy ethanol. The resultant solution was stirred at room temperature for more than 24 h to yield a clear, stable and homogeneous sol. The PH value of the sol was adjusted with nitric acid to 10, followed by hydrolysis and polycondensation by slowly adding water in the sol, the gel was dried at 120 °C to produce amorphous crystals, and the amorphous crystals were crushed into powders using a mortar and pestle. After the crushed powders were sieved by 120 meshes, the powders were calcinated at 500–850 °C using a 6 °C/min heating rate and soaked for 4 h. The NKBT powders which were in order of 80–200 nm were obtained.

The NKBT powders were ball milled for 4 h with the addition of 20–40 wt.% of organic vehicle. The organic vehicle usually consists of a binder (ethyl cellulose), a solvent (α-terpineol), a plasticizer (polyethylene glycol) and a dispersing agent (butoxyethoxyethyl acetate). After the ball milling, the viscosity of the prepared screen-printable pastes was measured by viscosimeter and adjusted in the range 20–80 Pa s for shear rate 18^{-1} s. NKBT layers were screen-printed with a 320 mesh screen mask on 96% alumina substrates (20 mm × 15 mm × 0.5 mm), which were first electroded with an Pt pastes. The bottom electrodes were produced on alumina substrates by a double print Pt screen printing process with Pt inks and then fired at 1250 °C for 30 min. The final electrode was about 5 μm with lateral dimensions of 15 mm × 15 mm. After each NKBT layer deposition, the wet layer was subsequently leveled for 15 min at room temperature, and then dried at 120 °C for 10 min. And then an uniaxial pressure of 50 MPa was applied on dried films to increase the green density and improve the densification of NKBT layers. In order to fire the organic vehicle the layers precalcined at 550 °C for 5 min with a heating rate of 180 °C/min in rapid thermal processor (RTP). The processes from printing to firing were repeated several times to obtain the required thickness of the NKBT films. The final firing of the piezoelectric thick films was performed at 1080–1160 °C for 30 min in air.

TG and DTA analysis for the dried NKBT screen pastes were carried out with Pyris Diamond TG/DTA thermogravimeter (Perkin-Elmer Instruments, USA) in dynamic nitrogen atmosphere and at a heating rate of 10 °C/min. The crystal phases of the powders and NKBT thick films were identified by powder X-ray diffraction obtained by a X'Pert PRO diffractometer (PANalytical B.V., the Netherlands) using Cu $K\alpha$ radiation (λ = 1.5406 Å) at voltage and current of 40 kV and 30 mA. XRD data were collected in the range of 20–60° in θ–2θ scanning mode with a 0.02° step and scanning speed of 5°/min. The Fourier transform infrared (FT-IR) spectrum of the samples was analyzed with Fourier transform infrared spectrometer (VERTEX 70, Bruker, Germany) equipped with a KBr beamsplitter and a photo-voltaic MCT detector. The surface micrograph of the NKBT powders and the thick films as well as the cross-section micrograph of the NKBT thick films were examined by field-emission scanning electron microscopy (FE-SEM, Sirion 200, FEI, USA). For dielectric, ferroelectric, and piezoelectric measurements, platinum top electrodes with diameters of 0.8 mm and thickness of 0.3 μm were sputtered onto the sintered NKBT layers. The NKBT thick films were poled by using 100–300 kV/cm applied field at 100 °C for 10 min in silicone oil. The films are short-circuited for 24 h after poling in order to allow the release of excess charges injected during the poling process. Dielectric performance measurements were performed using an LF impedance analyzer (Model HP 4192A, Hewlett-Packard, USA), a modified Sawyer-Tower circuit for ferroelectric hysteresis measurements, and a dual-beam laser interferometer for the longitudinal piezoelectric charge coefficient, d_{33eff} measurements.

3. Results and discussion

3.1. Sol–gel characteristics

Fig. 1 shows the FT-IR spectra of the NKBT precursors heat treated at 100 and 160 °C for 2 h. It can be seen that the peak located at around 3416.71 cm^{-1} is related to the stretching vibration of –OH group [21]. The peaks in the range of 1100–1000 cm^{-1} is corresponding to the C–O and C–O–C vibration. The strong bands at 615.91 and 615.93 cm^{-1} are assigned to Ti–O asymmetrical stretching vibration [22]. The peaks at 886.18, 794.89, and 662.22 cm^{-1} are related to stretching vibration of Bi–O, Na–O, and K–O, respectively. Moreover, the peaks at 1556.09 cm^{-1} and 1374.93 are correspond-

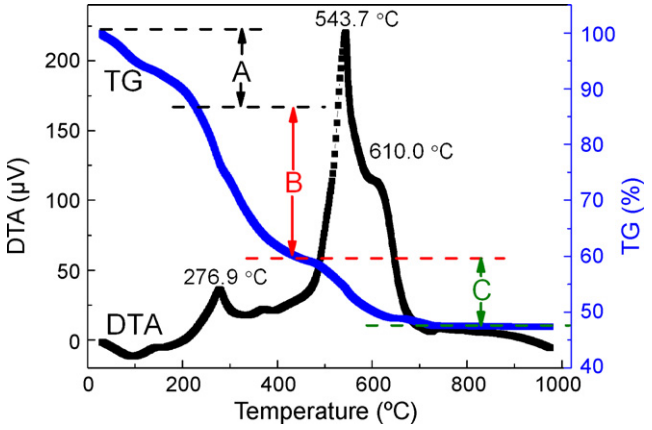

Fig. 2. TG–DTA curves of NKBT xerogel.

ing to asymmetrical stretching vibration $\nu_{as}(CO_2)$ and symmetric stretching vibration $\nu_s(CO_2)$ of $[COO]^-$ in the metal acetic complex [12], indicating that $Ti(OC_4H_9)_4$ reacted with CH_3COOH and CH_3COO^- replaced the $(OC_4H_9)^{-1}$ radical in $Ti(OC_4H_9)_4$. The peaks located at 1650.02, 1266.66, 886.18, and 662.22 cm^{-1} related to asymmetric stretching vibration and symmetric stretching vibration of NO_2 in nitrate esters, stretching vibration of NO_2–O, and bending vibration of NO_2, respectively. This implies that the sol has undergone esterification reactions as heated at 100 °C for 2 h. As shown in Fig. 1(b) the peak of carbonyl C=O disappeared when the sols heated at 160 °C for 2 h, which indicates that the nucleophilic reaction has accomplished. Furthermore, because the heat treatment temperature of 160 °C is higher than boiling temperature (130 °C) of glycol monoethyl ether, the intensity of some peaks of glycol monoethyl ether decreased after 2 h heat treatment.

3.2. Powders preparation and characteristics

TG and DTA analyses were performed to determine the vaporization temperature of various organic binders and burning temperature of organic after NKBT xerogel fired in air atmosphere. Fig. 2 illustrates the TG-DTA curves of NKBT xerogel in the range of 30–1000 °C. For TG curve, there are three pedestal sits of weight loss, the first one appears at about 200 °C, and it is due to the evaporation of water and part of organic solvent. The second pedestal sit of weight loss appears in the range of 220–400 °C, and it is caused by the decomposition of organic group and burning of part of the organic substances. The last pedestal sit of weight loss located in the range of 460–680 °C is resulted from the solid state reaction and the decomposition of nitrate materials such as $Bi(NO_3)_3$, sodium acetate or potassium acetate [23]. There is no weight loss above 650 °C. As shown in DTA curves, there are also three main exothermic peaks in the range of 30–1000 °C. The first exothermic peak appears at 276.9 °C which is regarded as the temperature of the decomposition and the burning of the organic substances. The second exothermic peak located at 543.7 °C is related to the formation of the perovskite phase due to the solid state reaction. The last one at 610.0 °C is caused by the secondary phase of pyrochlore changing to perovskite phase. These results are in perfect concordance with the XRD analysis of the NKBT xerogel calcined various temperatures. The XRD patterns are shown in Fig. 4. When the temperature is higher than 700 °C, the TG and DTA curves become very flat, which indicates that the NKBT perovskite phase has formed in the range of 460–700 °C. Moreover, from the analysis of Fig. 2,

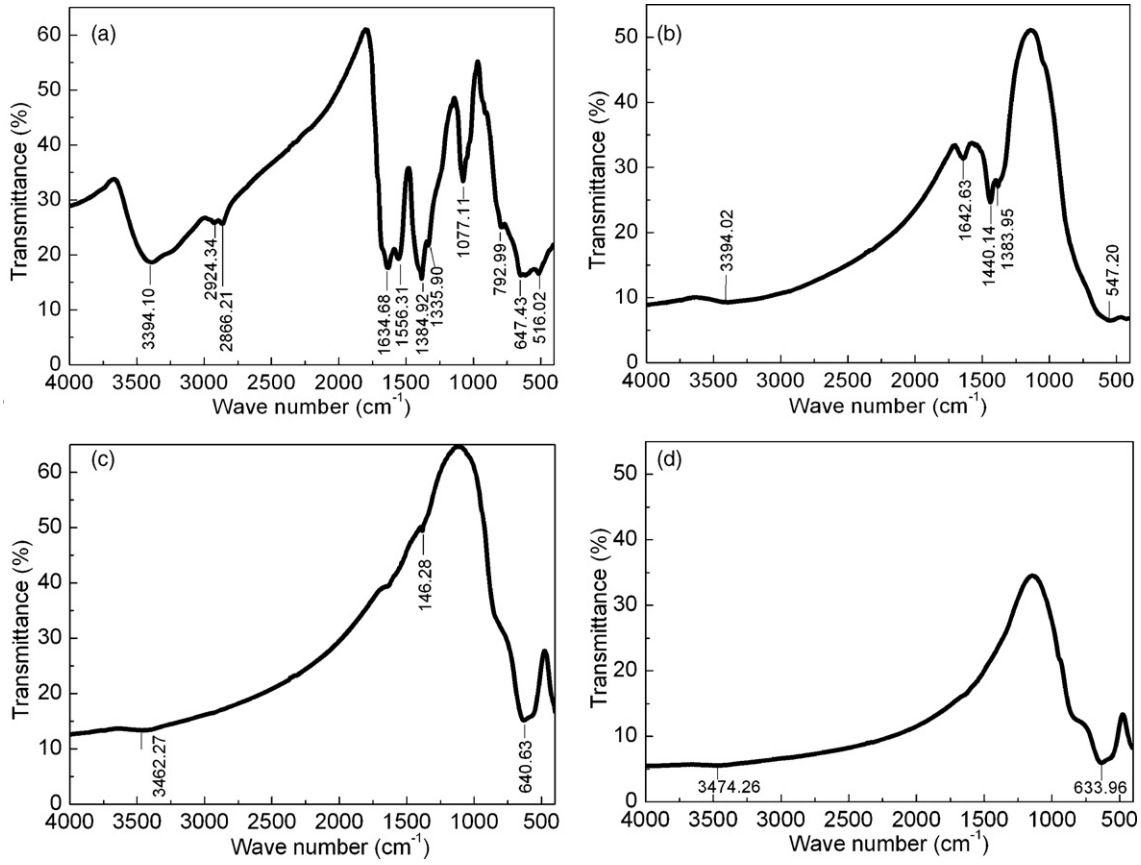

Fig. 3. FT-IR spectra of NKBT xerogel fired at different temperatures for 4 h (a) 200 °C, (b) 400 °C, (c) 550 °C, and (d) 750 °C.

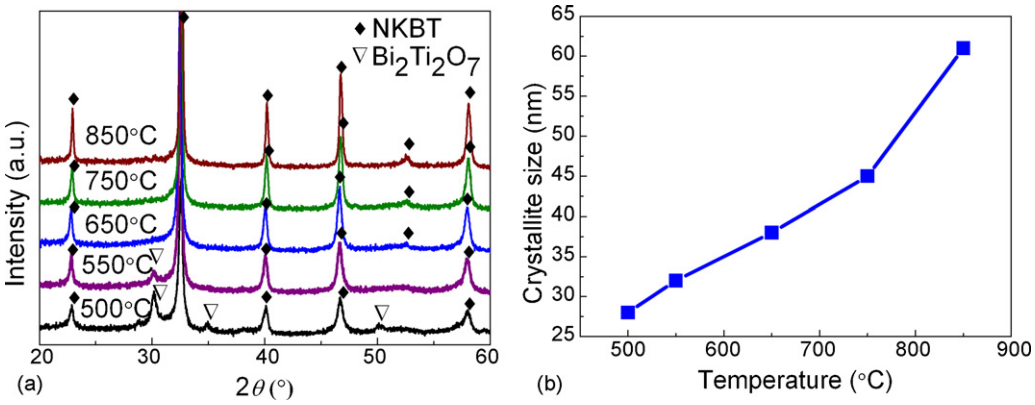

Fig. 4. XRD patterns (a) and crystalline size (b) of NKBT powders sintered at various temperatures for 4 h.

all combustion and decomposition of the materials as well as the crystallization of NKBT have finished by 700 °C.

The structure changes during the synthetic process were monitored by FT-IR analysis. Fig. 3 demonstrates the FT-IR spectra of the NKBT xerogel calcined at different temperatures. It can be seen that the peaks appearing at 3394 and 1634 cm^{-1} are related to the stretching vibration and the bending vibration of O–H bond [12] and the intensity of these two peaks gradually decrease with the increasing calcining temperature. The peaks located at 2924 and 2866 cm^{-1}, which corresponded to asymmetric stretching vibration and symmetric stretching vibration of CH_2. In addition, with the increases of the firing temperature of the xerogel, these two peaks disappeared after the temperature higher than 400 °C. As shown in Fig. 3(a), although the xerogel calcined at 200 °C for 2 h, the stretching vibration peak of associated –OH bond, stretching vibration peaks (1100–1000 cm^{-1}) of C–O and C–O–C bonds as well as the symmetric stretching vibration peak (1384 cm^{-1}) of O=C–O still can be observed. The stretching vibration peaks of $–NO_2$ and $–NH_2$ appears in the xerogel calcined at 400 °C as shown in Fig. 3(b). However, these peaks disappeared as the temperature increases to 550 °C, which is ascribed to the evaporation and burning temperature of C_3H_7NO. Moreover, as shown in Fig. 3(c) and (d) the intensity of the peak of Ti–O at 640 cm^{-1} increase with the increasing calcining temperature [12,22], indicating that the crystallinity increase with the firing temperature, which is consistent with the XRD analysis shown in Fig. 4.

XRD analysis was carried out to study the phase evolution of the xerogels in the calcination process. XRD patterns of xerogels calcined at 500, 550, 650, 750, and 850 °C are shown in Fig. 4. It can be seen that $Bi_2Ti_2O_7$ cubic pyrochlore phase as reported in the JCPDS File No. 32-0118 was formed at sintering temperature of 500 °C [24]. When the temperature increased to 550 °C, the

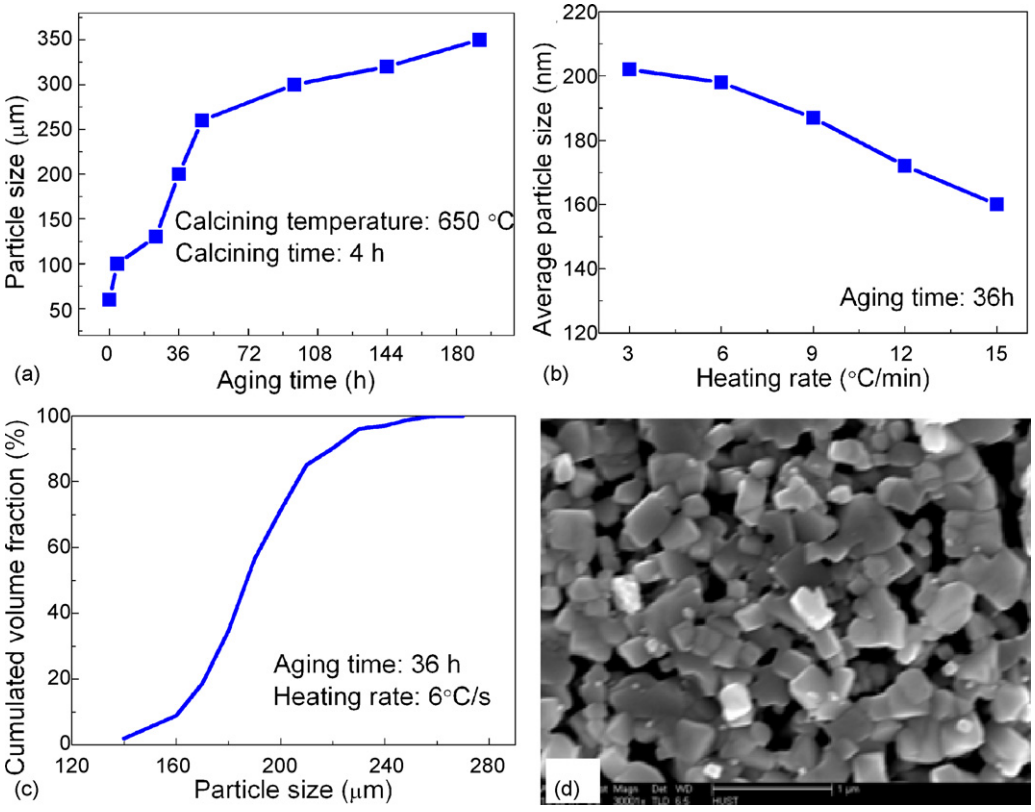

Fig. 5. Aging time dependence of particle size (a), heating rate dependence of average particle size (b), cumulated volume fraction (c), and SEM surface micrographs (d) of the NKBT powders.

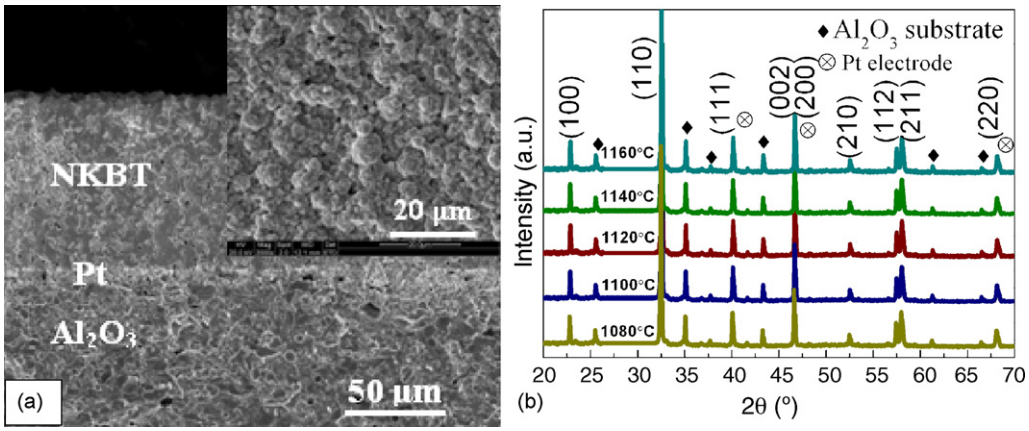

Fig. 6. Scanning electron microscopic cross-sectional and surface (the insert figure) micrographs (a), and X-ray diffraction (XRD) patterns (b) of the NKBT thick films.

height of the diffraction peaks belonging to $Bi_2Ti_2O_7$ decreased. It means that part of the $Bi_2Ti_2O_7$ cubic pyrochlore phase transform to perovskite phase as the powders calcined at 550 °C. When the temperature raised to 650 °C, all of the characteristic peaks of perovskite NKBT crystal appeared at 22.94°, 32.58°, 40.16°, 46.70°, 52.61°, and 58.02°, and all of the pyrochlore phase changed to perovskite phase. This transition temperature is lower than that of the KBT powders prepared by sol–gel method reported by Zhu et al. [25]. This can be attributed to the decrease of the forming temperature of the NKBT perovskite solid solution system caused by the addition of NBT to KBT. After further increasing of the temperature to 750 °C and above, only diffractions belonging to perovskite NKBT were observed and there was no evidence of a second phase. The full width at half maximum of the (1 0 1) diffraction peak of NKBT powders changed from 0.217° at 650 °C to 0.167° at 850 °C, respectively. It means that the average grain size increased from 48 to 71 nm according to Scherrer's equation.

It has been believed that the aging time of the sol strongly influences the particle size of the powders prepared by sol–gel method [26,27]. Fig. 5(a) shows the dependence of the average particle size of NKBT powders on aging time of precursor solution. The average particle size increases with the increasing aging time, when the NKBT precursor sol aged 36 h, the average particle size of 196 nm can be observed. The increased particle size can be attributed to polycondensation of the sol in the aging procedure. During this procedure the polymer cluster cross-linked to form bigger cluster, and the liquid phase were wrapped in the solid skeletons. Moreover, in this procedure the differences in curvature radius of the particle clusters can lead to its different solubility, resulting in different rates of growth of the cluster particles in the progress of Ostward ripening [28]. It is believed that chemical reaction-limited aggregation (RLA) was responsible for most of the sol aging, followed by diffusion-limited aggregation in the later stage [27]. Since the shape and size of NKBT powder present strong dependence on the aging time, the precursor solution must be aged for proper time evading inhomogeneous particle size resulting short aging time and oversize particle resulting from long time aging.

The heating rate also significantly influences the average particle size of NKBT powders. Fig. 5(b) illustrates the heating rate dependence of average particle size of the NKBT xerogel calcined at 650 °C for 4 h. It can be seen that the average particle size of NKBT powders decreases with the heating rate. This means that finer NKBT powder can be obtained from the xerogel calcined at certain temperature with a higher heating rate. However, the dwell time of 4 h is not enough for the formation of complete perovskite NKBT phases at the higher heating rate. Therefore, the relative low heating rate of 6 °C/min was chose for the calcining of NKBT powders at 650 °C for 4 h in present study. Fig. 5(c) and (d) demonstrates the cumulated volume fraction and SEM surface micrographs of the NKBT powders calcined at 650 °C for 4 h with the heating rate of 6 °C/min, respectively. It can be seen that cubic shape particulates with the order of 140–260 nm in size can be obtained from the xerogel calcined at 650 °C. Moreover, there is no obvious agglomeration of the NKBT powders, which is favourable for the preparation of NKBT screen printing pastes with optimal rheological properties.

3.3. Thick film preparation and characterization

Fig. 6 exhibits the scanning electron microscopic surface and cross-section micrographs of the NKBT thick films sintered at 1140 °C for 30 min, and the XRD patterns of the NKBT thick films sintered at 1080, 1100, 1120, 1140, and 1160 °C for 30 min. The NKBT thick films demonstrate a reasonably dense microstructure although there exits a small amount of pores resulting from the burning of the residual organic vehicle in green films as shown in Fig. 6(a). Moreover, the grain size of NKBT thick film is rather regular and without obvious presence of secondary phase. The grain size was approximately 1.1 μm, which was much larger than the grain in NKBT thin film [29]. The small grain size is caused not only by the rather short time for annealing process and low sintering temperature but also resulted from the constrained sintering by substrate. A slight interdiffusion between the NKBT film and the Pt/alumina substrate can be observed. The general mechanisms of densification and grain growth were similar in bulk samples and thick films, but the maximum of densification occurred at lower temperature for the thick films.

The NKBT thick films present the pure perovskite structures and the coexistence of rhombohedral and tetragonal MPB phases at room temperature are shown in Fig. 6(b). The high temperature sintering does not change the crystalline structure of NKBT thick films and no second phase was observed. The rhombohedral symmetry and tetragonal symmetry of the NKBT thick films at room temperature are characterized by a (0 0 2)/(2 0 0) peak splitting near 46° and a (2 1 1)/(1 1 2) peak splitting near 58°, respectively [30]. The existence of the MPB between rhombohedral NBT and tetragonal KBT phases of the NKBT thick films is beneficial to the high piezoelectric and ferroelectric properties. It is noteworthy that the XRD patterns still exhibit the splitting for the (2 0 0) and (2 1 1)/(1 1 2) peaks even the NKBT sintered at 1160 °C. This indicates that the symmetry of NKBT thick films did not become rhombohedral when the sintering temperature increased to 1160 °C. However, Zhang et al. [8] found that the perovskite structure transform from the coexistence of rhombohedral and tetragonal MPB phases to rhombohedral phase when the NKBT ceramics sintered at 1170 °C for 3 h.

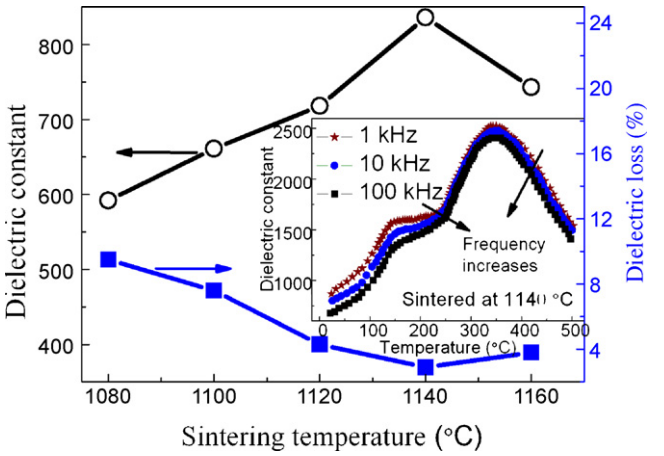

Fig. 7. Room-temperature dielectric properties (at 10 kHz) of NKBT thick films sintered at different temperatures, the insert figure shows the dielectric constant as functions of temperature at 1, 10, and 100 kHz.

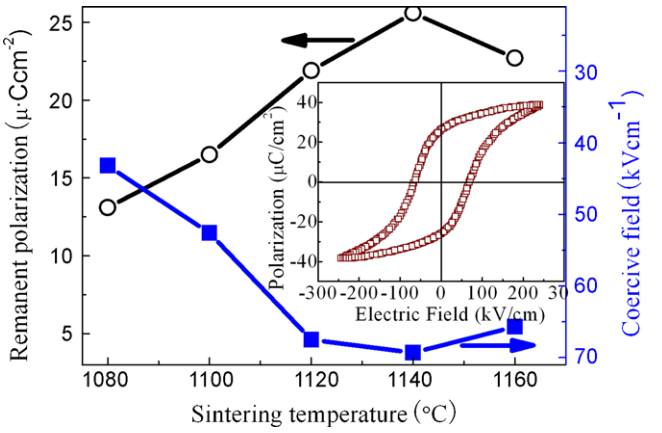

Fig. 8. Remanent polarization and coercive field of the NKBT thick films sintered at different temperatures, the insert figure shows the *P*–*E* loops of the NKBT thick films sintered at 1140 °C.

They attributed the phase transition to the accelerated volatilization of K element and the change of Na/K ratio of NKBT ceramics at higher sintering temperature (1170 °C). This implies that compared to the ceramics the relative shorter sintering-time for NKBT thick films would be propitious to maintain of the MPB phases and to improve of the electrical properties.

3.4. Dielectric properties

Fig. 7 shows the room-temperature dielectric properties (10 kHz) of NKBT thick films sintered at different temperatures. As the sintering temperature increases, the dielectric constant increases due to the improvement of the density with the sintering temperature, and the NKBT thick films sintered at 1140 °C exhibit the maximum dielectric constant of 836 and the minimum dielectric loss of 2.9%. This dielectric constant is higher than the dielectric constant of 703.5 of the PZW–PZT thick films deposited by screen printing [31] but is much lower than that of the NBT-based ceramics. Compared with the ceramics, the low-dielectric constant can be attributed to several effects, including a larger porosity of the films, clamping with the substrate, or interfacial layer between the film and bottom electrode. For PZT thick films, about 1/3 of dielectric constant bulk value is obtained by Simon et al. [32]. Compared to the NBT-based thin films, however, this dielectric constant is about twice higher than that reported for NBT–KBT15 thin film fabricated by sol–gel spin coating, which the highest dielectric constant of 360 is measured at 100 kHz [29]. It is noteworthy that the relatively high dielectric constant respect to that of conventional thin films just demonstrates the advantageous of piezoelectric thick films. As has been demonstrated by Xu et al. [33], there are both intrinsic and extrinsic contributions to the dielectric and ferroelectric responses of ferroelectric materials at room temperature. It is believed that about 25–50% of the dielectric response of ferroelectric films at room temperature was from extrinsic sources [33]. The extrinsic contribution to the dielectric constant of NKBT thick films was mainly related to 180° domain wall motion, which increased with the film thickness. This indicates that the enhanced domain wall activity is responsible for increased dielectric constant at room temperature as the NKBT film thickness increases. Moreover, because the thickness of the interfacial low-dielectric layer between film and substrate is supposed to be in dependent of the total film thickness [34], the decrease of the thickness ratio of interfacial layer to total thick films is also responsible for the high dielectric constant and low-dielectric loss of the NKBT thick films. The insert figure shows the dielectric constant as functions of temperature for NKBT thick films sintered at 1, 10, and 100 kHz.

The local maximum dielectric constant and dielectric loss locate at 130 °C (T_f) and 350 °C (T_m), respectively. A phase transition from the ferroelectric to the antiferroelectric phase for NKBT thick films is observed at about 130 °C, which is consistent with a previous report [6]. The remarkable increase of the dielectric constant at high temperature and low frequencies is significant of space charge polarization and associated ionic conductivity. The value of dielectric constant in the local maximum decreases and its temperature is shifted upward with frequency in a way similar to that observed for typical relaxor materials.

3.5. Ferroelectric properties

Fig. 8 illustrates the ferroelectric properties of NKBT thick films sintered at different temperatures. When the sintering temperature is lower than 1140 °C, the remanent polarization and the coercive field increase with the increasing sintering temperature, which is result from the increasing density with the sintering temperature. The optimal ferroelectric properties of the NKBT thick films sintered at 1140 °C reaches as high as 25.6 μC/cm^2 which is about two times larger than that of the NBT–KBT15 thin film (Pr = 13.8 μC/cm^2) [29]. Compared to conventional ferroelectric thin films (with thickness lower than 1 μm), the larger remanent polarization can be ascribed to the larger domain wall density and less domain wall pinning resulting from the increasing film thickness of NKBT thick films. Moreover, it can be seen from the insert figure that the NKBT thick film fired at 1140 °C shows a well-behaved and slight slanting shape hysteresis loops under an electric field of 0.2 MV/cm. The slight slanting shape of the loops could originate from a lateral clamping effect of the substrate during poling treatment. The coercive field of 69.3 kV/cm of the NKBT thick film is much higher than that in the NKBT bulk ceramics (about 25 kV/cm) [35]. The higher coercive field in thick film is probably determined by the conditions of domain nucleation at the surfaces of the film, which is different from the bulk ceramic. Compared with ceramics, owing to the dielectric nature of the interfacial layer between ferroelectric and electrode, the electric field within this layer is much larger than the average field throughout the film. Thus, the existing interfacial layer is responsible for the increase of the coercive filed Gao and Wang [36] also found that the existence of an interfacial dead layer, which leads to an increases in coercive field and a slight reduction in relative dielectric constant. Besides the interfacial layer and the depolarization field, the residual stress is also an important factor to influence the ferroelectric properties [37]. The comparatively large

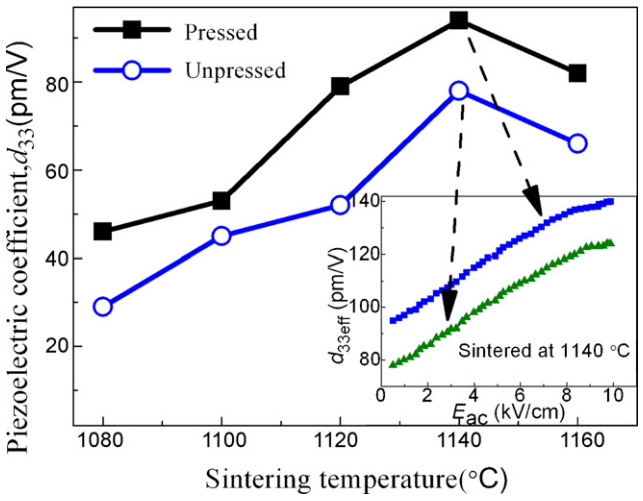

Fig. 9. Piezoelectric properties of the NKBT thick films sintered at different temperatures, the insert figure shows the longitudinal piezoelectric coefficient d_{33eff} of the NKBT thick films measured as a function of ac driving electric field amplitude at 5 kHz.

residual stress in the NKBT thick films could prohibit the domain wall motion and result in the increase of the coercive field of the films.

3.6. Piezoelectric properties

As shown in Fig. 9, the effective longitudinal piezoelectric coefficient d_{33eff} increases with the sintering temperature, this is result from the increasing density. Moreover, the piezoelectric coefficient of the pressed NKBT thick films is larger than that of the unpressed NKBT thick films, indicating that the applying axial press is an efficient method to improve the density and the piezoelectric properties of the screen printing thick films. It can be seen that the pressed NKBT thick films sintered at 1140 °C exhibit excellent piezoelectric properties with an effective longitudinal piezoelectric coefficient d_{33eff} of 95 pm/V. This value is much higher than that of the PZT thin films [38]. There have been several reports that effective d_{33eff} increases with film thickness [33,39]. The increased contribution of non-180° domain wall motion with increasing film thickness is used as a general statement for submicron films. The effective longitudinal of piezoelectric thick films have been measured to be much smaller that those of their bulk counterparts. Two main factors are considered to be responsible for this, one is the clamping effect of the substrate and the other is limited extrinsic contributions to the piezoelectric properties due to the inability to activate the non-180° domain wall motion. The clamping by substrate and the pining of the domain wall could be weakened due to the increased film thickness [40]. Therefore, the reduced clamping effect and the enhanced domain wall motion were liable for the increase of the effective longitudinal piezoelectric coefficient with increasing film thickness.

The insert figure shows the longitudinal piezoelectric coefficient d_{33eff} of the NKBT thick films measured as a function of ac driving electric field amplitude at 5 kHz. The strong field dependence of d_{33eff} suggests active contribution of non-180° domain walls in the film [41]. The effective longitudinal piezoelectric coefficients d_{33eff} of the pressed and unpressed NKBT thick film at zero bias are around 95 and 78 pm/V, respectively. This value is comparable to that in PZT thick films produced by screen printing [42]. It has been reported for a number of ferroelectric ceramics and thin films that the piezoelectric coefficient increased with the increasing the applied field's amplitude when the applied field beyond a certain threshold field E_{th} [43,44]. The longitudinal piezoelectric coefficient becomes a function of the applied field's amplitude, which are usually referred to as piezoelectric nonlinearity. The linear dependence of the longitudinal piezoelectric coefficient on the applied ac electric field indicates domain wall contribution to the polarization and piezoelectric strain, as observed in bulk ceramics [41].

4. Conclusions

NKBT lead-free thick films have been successfully deposited on Pt electroded alumina substrate using screen printing from the sol–gel derived powders. In this study, the sol–gel process was employed to prepare NKBT powders at lower temperature for limiting the loss of volatile Bi_2O_3, K_2O and Na_2O. The transition mechanism of NKBT sol to gel was studied. Moreover, the effects of aging time, calcining temperature, dwell time, and heating rate on NKBT particle size and particle shape were system investigated. Our results demonstrate that part of the $Bi_2Ti_2O_7$ cubic pyrochlore phase transform to perovskite phase as the powders calcined at 550 °C. When the temperature increases to 650 °C, all of the characteristic peaks of perovskite NKBT crystal appeared at 22.94°, 32.58°, 40.16°, 46.70°, 52.61°, and 58.02°, and all of the pyrochlore phase changed to perovskite phase. The average particle size increases with the increasing aging time, when the NKBT precursor sol aged 36 h, NKBT with the average particle size of 196 nm can be observed. Furthermore, the cubic shape particulates of the order of 140–260 nm in size can be obtained from the xerogel calcined at 650 °C, and there is no obvious agglomeration of the NKBT powders, which is favourable for the preparation of NKBT screen printing pastes with optimal rheological properties.

In addition, the dielectric, ferroelectric and piezoelectric properties of the NKBT thick films sintered at various temperatures were studied. Our results show that the dielectric constant, remanent polarization, and longitudinal piezoelectric coefficient of NKBT thick films increased with the increasing sintering temperature due to the improvement of the density with the sintering temperature. Moreover, compared to conventional ferroelectric thin films, the improvement of the electric properties can be attributed to the larger domain wall density and less domain wall pinning resulting from the increasing film thickness of NKBT thick films. The resulting typical 90 μm thick films exhibit relative dielectric constant of 836 (at 10 kHz), dielectric constant of 2.9%, remnant polarization of 25.6 μC/cm^2, coercive field of 69.3 kV/cm, and longitudinal effective piezoelectric coefficient, d_{33eff} of 95 pm/V. Compared with NBT-based piezoelectric ceramics, the smaller longitudinal piezoelectric coefficient results from the clamping effect of the substrate and the limited extrinsic contributions to the piezoelectric properties due to the inability to activate the non-180° domain wall motion. However, the performance of these NKBT lead-free piezoelectric thick films could comparable to the lead based piezoelectric thick films. The thick films are expected to be a new and promising candidate for lead-free piezoelectric micro-devices especially the micro-actuators applications. In addition, this work furthers the understanding the mechanism of sol–gel derived perovskite ferroelectric powders and screen printing processing from sol–gel derived powders of piezoelectric thick films.

Acknowledgements

This research was partially supported by China Postdoctoral Science Foundation (No. 20090460933), National High Technology Research and Development Program of China (No. 2007AA03Z120), and the National Natural Science Foundation of China (No. 60777043).The authors also wish to thank the Analytical and Testing Center of Huazhong University of Science and Technology for SEM, XRD, and FTI-IR analysis.

References

[1] Y. Saito, H. Takao, T. Tani, T. Nonoyama, K. Takatori, T. Homma, T. Nagaya, M. Nakamura, Nature 432 (2004) 84–87.
[2] G. Smolenskii, V. Isupov, A. Agranovskaya, N. Krainik, Sov. Phys. Solid State 2 (1961) 2651–2654.
[3] H. Nagata, T. Takenaka, Jpn. J. Appl. Phys. 36 (1997) 6055–6057.
[4] H. Nagata, T. Shinya, Y. Hiruma, T. Takenaka, I. Sakaguchi, H. Haneda, Ceram. Trans. 167 (2005) 213–221.
[5] H. Nagata, M. Yoshida, Y. Makiuchi, T. Takenaka, Jpn. J. Appl. Phys. 42 (2003) 7401–7403.
[6] V.A. Isupov, Ferroelectrics 315 (2005) 123–147.
[7] J. Shieh, K.C. Wu, C.S. Chen, Acta Mater. 55 (2007) 3081–3087.
[8] Y.R. Zhang, J.F. Li, B.P. Zhang, J. Am. Ceram. Soc. 91 (2008) 2716–2719.
[9] A. Sasaki, T. Chiba, Y. Mamiya, E. Otsuki, Jpn. J. Appl. Phys. 38 (1999) 5564–5567.
[10] H.B. Zhang, S.L. Jiang, Y.K. Zeng, Appl. Phys. Lett. 92 (2008) 152901.
[11] H.B. Zhang, S.L. Jiang, J. Eur. Ceram. Soc. 29 (2009) 717–723.
[12] E. Mercadelli, C. Galassi, A.L. Costa, S. Albonetti, A. Sanson, J. Sol–gel. Sci. Technol. 46 (2008) 39–45.
[13] Y.J. Ma, J.H. Cho, Y.H. Lee, B.I. Kim, Mater. Chem. Phys. 98 (2006) 5–8.
[14] J. Hao, X. Wang, R. Chen, L. Li, Mater. Chem. Phys. 90 (2005) 282–285.
[15] H.A.M. Van Hal, W.A. Groen, S. Maassen, W.C. Keur, J. Eur. Ceram. Soc. 21 (2001) 1689–1692.
[16] R.A. Dorey, R.W. Whatmore, J. Electroceram. 12 (2004) 19–32.
[17] R.N. Torah, S.P. Beeby, M.J. Tudor, N.M. White, J. Electroceram. 19 (2007) 95–110.
[18] D.A. Barrow, T.E. Petroff, R.P. Tandon, M. Sayer, J. Appl. Phys. 81 (1997) 876–881.
[19] A. Sen, P. Pramanik, J. Eur. Ceram. Soc. 21 (2001) 745–750.
[20] Y. Hao, Q. Lai, Z. Xu, X. Liu, X. Ji, Solid State Ionics 176 (2005) 1201–1206.
[21] T.I. Chang, J.L. Huang, H.P. Lin, S.C. Wang, H.H. Lu, L. Wu, J.F. Lin, J. Alloys Compd. 414 (2006) 224–229.
[22] S. Musić, M. Gotić, M. Ivanda, S. Popović, A. Turković, R. Trojko, A. Sekulić, K. Furić, Mater. Sci. Eng. 47 (1997) 33–40.
[23] C.Y. Kim, T. Sekino, K. Niihara, J. Am. Ceram. Soc. 86 (2003) 1464–1467.
[24] A.L. Hector, S.B. Wiggin, J. Solid State Chem. 177 (2004) 139–145.
[25] M. Zhu, L. Hou, Y. Hou, J. Liu, H. Wang, H. Yan, Mater. Chem. Phys. 99 (2006) 329–332.
[26] Q. Zhang, Z. Huang, R.W. Whatmore, J. Sol–gel. Sci. Technol. 23 (2002) 135–144.
[27] Z. Huang, Q. Zhang, R.W. Whatmore, J. Sol–gel. Sci. Technol. 24 (2002) 49–55.
[28] R. Takahashi, S. Sato, T. Sodesawa, M. Kawakita, K. Ogura, J. Phys. Chem. B 104 (2000) 12184–12191.
[29] T. Yu, K.W. Kwok, H.L.W. Chan, Mater. Lett. 61 (2007) 2117–2120.
[30] M. Zhu, L. Liu, Y. Hou, H. Wang, H. Yan, J. Am. Ceram. Soc. 90 (2007) 120–124.
[31] T.Y. Kwon, J.H. Park, Y.B. Kim, D.S. Yoon, C.I. Cheon, H.L. Lee, T.S. Kim, J. Cryst. Growth 295 (2006) 172–178.
[32] L. Simon, S. Le Dren, P. Gonnard, J. Eur. Ceram. Soc. 21 (2001) 1441–1444.
[33] F. Xu, S. Trolier-McKinstry, W. Ren, B. Xu, Z.L. Xie, K.J. Hemker, J. Appl. Phys. 89 (2001) 1336.
[34] A.K. Tagantsev, M. Landivar, E. Colla, N. Setter, J. Appl. Phys. 78 (1995) 2623–2630.
[35] Y.R. Zhang, J.F. Li, B.P. Zhang, C.E. Peng, J. Appl. Phys. 103 (2008) 074109.
[36] X.S. Gao, J. Wang, J. Appl. Phys. 99 (2006) 074103.
[37] Y. Jeon, D.G. Kim, K. No, S.J. Kim, J. Chung, Jpn. J. Appl. Phys. 39 (2000) 2705–2709.
[38] D.V. Taylor, D. Damjanovic, Appl. Phys. Lett. 76 (2000) 1615–1617.
[39] D.J. Kim, J.H. Park, D. Shen, J.W. Lee, A.I. Kingon, Y.S. Yoon, S.H. Kim, Ceram. Int. 34 (2008) 1909–1915.
[40] R.N. Torah, S.P. Beeby, N.M. White, J. Phys. D. Appl. Phys. 37 (2004) 1074–1078.
[41] D. Damjanovic, J. Appl. Phys. 82 (1997) 1788–1797.
[42] E.S. Thiele, D. Damjanovic, N. Setter, J. Am. Ceram. Soc. 84 (2001) 2863–2868.
[43] N. Bassiri-Gharb, I. Fujii, E. Hong, S. Trolier-McKinstry, D. Taylor, D. Damjanovic, J. Electroceram. 19 (2007) 47–65.
[44] S. Li, W. Cao, L.E. Cross, J. Appl. Phys. 69 (1991) 7219–7224.